Journal of Engineering Science and Technology
Vol. 6, No. 4 (2011) 445 - 458

AN EFFICIENT HYDRODYNAMIC NUMERICAL MODEL WITH WETTING-DRYING CAPABILITY

PURWANTO BEKTI SANTOSO[1,*], NASTAIN[1], WAHYU WIDIYANTO[1], SUSUMU KANAYAMA[2], HITOSHI TANAKA[3]

[1]Department of Civil Engineering, Universitas Jenderal Soedirman, Jl. Mayjen Sungkono Km 5 Blater Purbalingga 53371, Jawa Tengah, Indonesia
[2]PENTA-OCEAN Institute of Technology, Tochigi, 329-2746, Japan
[3]Department of Civil Engineering, Tohoku University, Sendai, 980-8579, Japan
*Corresponding Author: purwanto@unsoed.ac.id

Abstract

The capability of a semi-implicit three-dimensional shallow water flow numerical model is extended by implementation of a wetting-drying scheme. The numerical model of the shallow water flow is examined in detail to reveal its inherent capability in simulating the wetting-drying process. In the implementation of a wetting drying scheme, a cell is defined as a dry cell, only if all the four depths at all of its sides become lower than a user defined threshold value. The greatest of the water levels computed in the center of two adjacent cells is taken as the water level at their common side, with a minimum value is specified for the resulting depth. The scheme was tested by comparisons between the model results and the analytical results of land-ocean interface position of linearly changed bottom-depth cases. The tests show excellent agreement between both of the results. Application to Segara Anakan was also carried out and shows the model capability in simulating the real condition.

Keywords: Shallow water flow, Numerical method, Finite difference method, Wetting-drying scheme.

1. Introduction

Water in a natural or a man-made water body tends to experience quality degradation. Water quality degradation causes less water available for the people and organic matters live in it. Human intervention to the environment, which changes the flow pattern, is mostly the cause of the water degradation. The change of flow pattern will cause formation of a new equilibrium state and will result in

Nomenclatures

A	Scaled tidal amplitude
C_D	Drag coefficient
G	Gravity, m/s^2
H	Total water depth measured from the bottom, m
H_{dry}	Minimum depth to be considered as a dry point, m
h	Water depth measured form still water level, m
i	Cells index in the horizontal x
j	Cells index in the horizontal y
k	Cells index in the vertical z
L_{EX}	Vertical index of the bottom layer
L_{SX}	Vertical index of the top layer
n	Numerical time step index
S_{HX}	Thickness of vertical flux faces in x-direction, m
S_{HY}	Thickness of vertical flux faces in y-direction, m
T	Scaled tidal period
t	Scaled time
u	Velocity in x-direction, m/s
u'	Scaled velocity of the moving land-ocean interface
v	Velocity in y-direction, m/s
w	Velocity in z-direction, m/s
x	Horizontal coordinate, m
y	Horizontal coordinate, m
z	Vertical coordinate, m

Greek Symbols

η	Scaled free surface elevation from the mean.
μ	Eddy viscosity in the horizontal, Ns/m^2
ν	Eddy viscosity in the vertical, Ns/m^2
θ_1	Degree of implicitness in numerical formulation
τ_x^w	Prescribed wind stresses in x-direction, N/m^2
τ_y^w	prescribed wind stresses in y-direction, N/m^2
ζ	Free water surface elevation, m

development of stagnation regions, relocation of pollutant and suspended sediment, and the ecologically impacted water body. Therefore, the physical representation, i.e., the flow pattern, is required as part of ecological modeling [1]. Good understanding of the physical process in a water body will be a basis in a water quality improvement strategy.

Many three dimensional numerical models of shallow water flow, for example POM [2], ROMS [3], SEOM [4] and many others, consider fix land-ocean boundary. The fixed boundary is based on assumption that there is a vertical wall blocking the seawater so that it will not pass through the boundary and reach the upper land. The fixed boundary condition can be implemented as long as the flow simulation is conducted over a wide region with neglected wetting-drying area and the main interest is on regions far from the boundary. For a region with mild slope and large change of inundation area between high tide and low tide, the wetting-drying condition, which enables the movement of land-ocean boundary, should be applied.

Attempts to implement the wetting-drying condition to the existing available shallow water flow numerical model have been found in literatures. Oey [5, 6] implemented a wetting-drying scheme into a terrain following finite difference hydrodynamic numerical model. Another work implemented the wetting-drying condition into a finite element hydrodynamic model [7, 8]. Basically, the above mentioned studies and many others implemented a wetting-drying scheme into a numerical solution of shallow-water equations that is not inherently capable of simulating the wetting-drying process. The incapability means that the wetting-drying scheme can not be implemented to the existing looping structure of the numerical solution [5-8]. Different looping structure of the wetting-drying scheme should be added to the existing numerical solution. Therefore, an additional computational burden and the mass-conservation problem usually arises [9].

To solve the three-dimensional shallow water flow equations, Sato et al. [10] made improvement in the solution of the linear system of equations resulted from semi-implicit discretation in Casulli and Cheng [11]. It results in more efficient computation because less matrix computation is involved, and has been found to work well in numerical studies of estuary and its environment [12, 13]. The original model of Casulli and Cheng [11] is inherently capable of simulating the wetting-drying process and free from mass-conservation problem. However, in Sato et al. [10], the implementation of the wetting-drying condition is not discussed and it is not known whether it has inherent capability of simulating the wetting-drying condition as in the original model [11].

In this paper, detail examination of the Sato's model is carried out to reveal its inherent capability in simulating the wetting-drying condition. The wetting-drying scheme implemented is the one from Casulli and Cheng [11], which uses the water level upstreaming resulting in more stable and smooth behavior of the water level and the flow velocity [14]. In this method, a cell is defined as a dry cell, only if all the four depths at its sides become lower than a user defined threshold value. The greatest between two water levels computed at the centers of adjacent cells is taken as the water level at their common side, with a minimum value is specified to the resulting depth.

2. The Governing Equation

Water flow in oceans, lakes, and rivers can be modelled by a mathematical expression known as Navier-Stoke equations. However, in practical implementation, the equations are simplified according to the characteristic of the problem considered. For the shallow water flow problem, the equations are simplified by the hydrostatic assumption by which the pressure terms can be approximated by the water depth. Furthermore, effect of turbulent can be represented by turbulent diffusion terms through the Boussinesq assumption. The shallow water flow equations can be written as follows

$$\frac{\partial u}{\partial t}+u\frac{\partial u}{\partial x}+v\frac{\partial u}{\partial y}+w\frac{\partial u}{\partial z}+g\frac{\partial \zeta}{\partial x}=\mu\left(\frac{\partial^2 u}{\partial x^2}+\frac{\partial^2 u}{\partial y^2}\right)+\nu\frac{\partial^2 u}{\partial z^2} \tag{1}$$

$$\frac{\partial v}{\partial t}+u\frac{\partial v}{\partial x}+v\frac{\partial v}{\partial y}+w\frac{\partial v}{\partial z}+g\frac{\partial \zeta}{\partial y}=\mu\left(\frac{\partial^2 v}{\partial x^2}+\frac{\partial^2 v}{\partial y^2}\right)+\nu\frac{\partial^2 v}{\partial z^2} \tag{2}$$

$$\frac{\partial u}{\partial x}+\frac{\partial v}{\partial y}+\frac{\partial w}{\partial z}=0 \tag{3}$$

In which, (u, v, w) are flow velocity in the direction of (x, y, z); ζ is free water surface elevation; g is the gravity; μ and ν are eddy viscosity in horizontal and vertical direction respectively. There four unknown variables, i.e., u, v, w, and ζ, therefore one more equation is required, i.e., the depth integration of the continuity equations with kinematics boundary condition at the water surface

$$\frac{\partial \zeta}{\partial t}+\frac{\partial}{\partial x}\left(\int_{-h}^{\zeta} u dz\right)+\frac{\partial}{\partial y}\left(\int_{-h}^{\zeta} v dz\right)=0 \tag{4}$$

In this expression, $h(x, y)$ is the water depth measured form still water level. Some numerical solution methods of the Eqs. (1) – (4) are, for example, the finite difference [2], the finite volume [15], and the finite element [16, 17]. Until to date, the finite difference method with the Arakawa C-grids [18], which is used in this study, is the most popular method.

3. Boundary Conditions

The shallow water flow equations include expressions which describe the stresses at lateral surfaces due to external forces. On the water surface wind stress causes a motion of the water but at the bottom the stress leads to decay of motion, and mathematically they act as water surface and bottom boundary conditions respectively. Theoretically both have the same form

$$\nu\frac{\partial u}{\partial z}=\tau, \qquad \nu\frac{\partial v}{\partial z}=\tau \tag{5}$$

They depend on the eddy viscosity and the vertical gradient of velocity, but their empirical forms differ strongly. The measurements of the bottom stress run already for many years under the different flow conditions and showed that the bottom stress is proportional to the square of the average velocity [19]

$$\nu\frac{\partial u}{\partial z}=C_D u\sqrt{u^2+v^2}, \qquad \nu\frac{\partial v}{\partial z}=C_D v\sqrt{u^2+v^2} \tag{6}$$

where C_D is the drag coefficient. The prescribed wind stresses, τ_x^w and τ_x^w, are applied at the free surface, which result in the following equations for the free surface boundary conditions

$$\nu\frac{\partial u}{\partial z}=\tau_x^w, \qquad \nu\frac{\partial v}{\partial z}=\tau_y^w \tag{7}$$

Experiments show that the wind stress is a function of wind velocity and the aerodynamic properties of the sea surface. Practical formulation is usually in the quadratic forms of wind speed [19].

In the horizontal at the land-water interface, the velocity component normal to the boundary is suppressed to have zero value whereas frictionless boundary condition is applied for the tangential velocity. Because of staggered grid implementation in the numerical solution, the boundary condition at the open sea usually is in the form of the water level. The implementation of the staggered grid allows separate calculation of the flow velocities and the water level, and therefore results in simpler calculation.

4.Numerical Discretization

Top view of the variables arrangement in a horizontal grid is shown in Fig. 1, whereas that of the vertical grid is shown in Fig. 2. Indices of i, j, and k represent cells numbering in the horizontal (x, y) and the vertical (z) respectively. Vertical layers numbering is carried out consecutively from the water surface to the bottom. In Fig. 1, L_{SX} and L_{EX} are the vertical numbering of the top and the bottom layers respectively at a horizontal grid. Number of effective layers at each horizontal location is different depending on its depth. Vertical flux faces of the same layer numbering can differ in their thickness because of the water level fluctuation and the water depth. Thickness of vertical flux faces in the direction of i and j are denoted as $S_{HX\,k,i,j}$ and $S_{HY\,k,i,j}$ respectively. According to Griffies [20], definitions of the vertical coordinate and the bottom representation are classified as the Z-model with partial-cell approximation for the bottom representation.

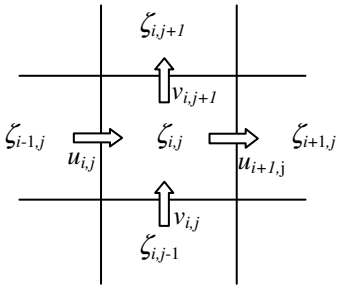

Fig. 1. Horizontal Arrangement of the Flow Variables.

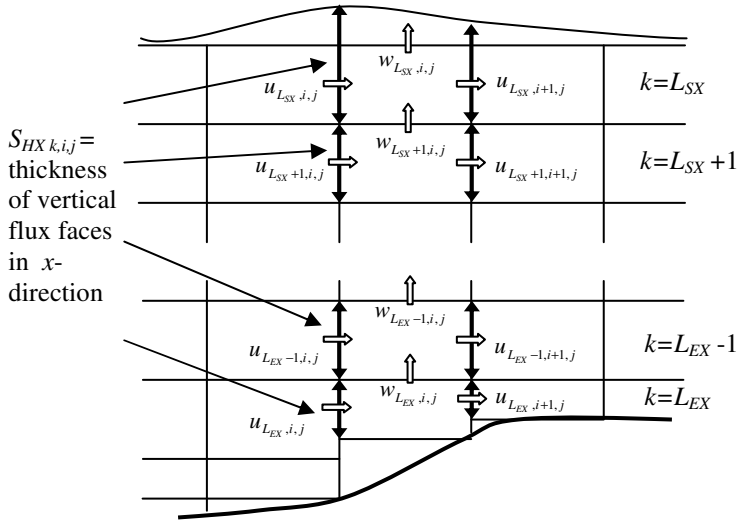

Fig. 2. Vertical Arrangement of the Flow Variables.

Steps of calculation are shown in Fig. 3. Basically, the steps include calculation of the water level, the horizontal flow velocities, and the vertical flow velocity. At the first step, the horizontal x-direction of the momentum equation can be written as follows

$$\frac{u^{n+1}-u^n}{\Delta t}+(u\frac{\partial u}{\partial x})^n+(v\frac{\partial u}{\partial y})^n+w^n(\frac{\partial u}{\partial z})^n+\theta_1 g(\frac{\partial \zeta}{\partial x})^{n+1}+(1-\theta_1)g(\frac{\partial \zeta}{\partial x})^n$$
$$=\nu_h\left(\frac{\partial^2 u}{\partial x^2}+\frac{\partial^2 u}{\partial y^2}\right)^n+\theta_1\{\frac{\partial}{\partial z}(\nu_v\frac{\partial u}{\partial z})\}^{n+1}+(1-\theta_1)\{\frac{\partial}{\partial z}(\nu_v\frac{\partial u}{\partial z})\}^n \quad (8)$$

The terms and variables with the superscript n are known from the calculation at the previous time step, whereas the superscript n+1 shows the ones that will be calculated. In Eq. (8), θ_1 is denoted as the degree of implicitness, which increases the computation stability as θ_1 is adjusted within the range of 0.5-1.0.

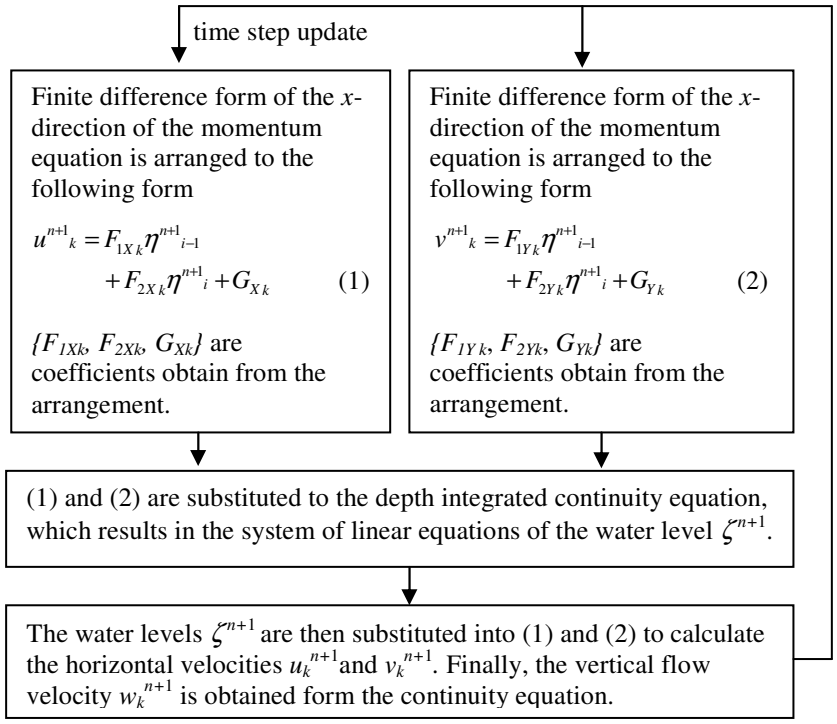

Fig. 3. Steps of Calculation.

The x-direction of the momentum equation of the k layer is written in the following form

$$-a_k u^{n+1}{}_{k-1}+b_k u^{n+1}{}_k-c_k u^{n+1}{}_{k+1}=d_{1k}\zeta^{n+1}{}_{i-1}+d_{2k}\zeta^{n+1}{}_i+e_k \quad (9)$$

where a, b, c, d_1, and d_2 are coefficients resulted form the implicit discretization of the equation, whereas e is resulted from discretization the explicit term. Equation (9) is a tridigional system of linear equations u^{n+1} that is coupled with the water level ζ^{n+1}. Application of the Thomas algorithm (forward and backward sweep) will further simplify the equation to the following form

$$u^{n+1}{}_k = F_{1Xk}\zeta^{n+1}{}_{i-1}+F_{2Xk}\zeta^{n+1}{}_i+G_{Xk} \quad (10)$$

in which F_{1Xk}, F_{2Xk}, and G_{Xk} are obtained from

$$F_{1Xk}=R_k F_{1Xk+1}+S_{1k} \quad (11)$$

$$F_{2X\,k} = R_k F_{2X\,k+1} + S_{2k} \tag{12}$$

$$G_{X\,k} = R_k G_{X\,k+1} + T_k \tag{13}$$

for $k=L_{EX}$-1 to $k=L_{SX}$. For the bottom layer $k=L_{EX}$, the calculation is based from

$$F_{1X\,L_{EX}} = \frac{d_{1L_{EX}} + a_{L_{EX}} S_{1L_{EX}-1}}{b_{L_{EX}} - a_{L_{EX}} R_{L_{EX}-1}} \tag{14}$$

$$F_{2X\,L_{EX}} = \frac{d_{2L_{EX}} + a_{L_{EX}} S_{2L_{EX}-1}}{b_{L_{EX}} - a_{L_{EX}} R_{L_{EX}-1}} \tag{15}$$

$$G_{X\,L_{EX}} = \frac{e_{L_{EX}} + a_{L_{EX}} T_{L_{EX}-1}}{b_{L_{EX}} - a_{L_{EX}} R_{L_{EX}-1}} \tag{16}$$

The coefficients of R_k, S_{1k}, S_{2k}, T_k are previously defined from the forward-sweep $k=L_{SX}+1$ to $k=L_{EX}$ -1 using the equations

$$R_k = \frac{c_k}{(b_k - a_k R_{k-1})} \tag{17}$$

$$S_{1k} = \frac{d_{1\,k} + a_k S_{1\,k-1}}{(b_k - a_k R_{k-1})} \tag{18}$$

$$S_{2k} = \frac{d_{2\,k} + a_k S_{2\,k-1}}{(b_k - a_k R_{k-1})} \tag{19}$$

$$T_k = \frac{a_k T_{k-1} + e_k}{(b_k - a_k R_{k-1})} \tag{20}$$

At the surface layer, $k=L_{SX}$, the coefficients are obtained from

$$R_{L_{SX}} = \frac{c_{L_{SX}}}{b_{L_{SX}}} \tag{21}$$

$$S_{1L_{SX}} = \frac{d_{1L_{SX}}}{b_{L_{SX}}} \tag{22}$$

$$S_{2L_{SX}} = \frac{d_{2L_{SX}}}{b_{L_{SX}}} \tag{23}$$

$$T_{L_{SX}} = \frac{e_{L_{SX}}}{b_{L_{SX}}} \tag{24}$$

For the y-direction, discretization of the momentum equation will result in the form of

$$v^{n+1}{}_k = F_{1Y\,k}\,\zeta^{n+1}{}_{i-1} + F_{2Y\,k}\,\zeta^{n+1}{}_i + G_{Y\,k} \tag{25}$$

where F_{1Yk}, F_{2Yk}, and G_{Yk} are obtain similarly as in Eqs. (11)-(24).

The depth integrated of the continuity equation, i.e., Eq. (4), is discretized to get the following form

$$\zeta^{n+1}{}_{i,j} - \zeta^{n}{}_{i,j} + \frac{\theta_1 \Delta t}{\Delta x} \sum u^{n+1}{}_{k,i+1,j} S_{HX\,k,i+1,j} - \frac{\theta_1 \Delta t}{\Delta x} \sum u^{n+1}{}_{k,i,j} S_{HX\,k,i,j}$$

$$+\frac{\theta_1\Delta t}{\Delta y}\sum v^{n+1}{}_{k,i,j+1}S_{HY\,k,i,j+1}-\frac{\theta_1\Delta t}{\Delta y}\sum v^{n+1}{}_{k,i,j}S_{HY\,k,i,j}$$
$$+\frac{(1-\theta_1)\Delta t}{\Delta x}\sum u^{n}{}_{k,i+1,j}S_{HX\,k,i+1,j}-\frac{(1-\theta_1)\Delta t}{\Delta x}\sum u^{n}{}_{k,i,j}S_{HX\,k,i,j}$$
$$+\frac{(1-\theta_1)\Delta t}{\Delta y}\sum v^{n}{}_{k,i,j+1}S_{HY\,k,i,j+1}-\frac{(1-\theta_1)\Delta t}{\Delta y}\sum v^{n}{}_{k,i,j}S_{HY\,k,i,j}=0 \quad (26)$$

where Σ is summation from $k=L_{SX}$ to $k=L_{EX}$. The variables of horizontal velocity ($u^{n+1}{}_k$, $v^{n+1}{}_k$) in the above equation are eliminated by substituting Eqs. (10) and (25). The elimination results in a system of linear equations

$$a_{ij}\zeta_{i-1,j}+b_{ij}\zeta_{ij}+c_{ij}\zeta_{i+1,j}+d_{ij}\zeta_{i,j-1}+e_{ij}\zeta_{i,j+1}=f_{ij} \quad (27)$$

a_{ij}, b_{ij}, c_{ij}, d_{ij}, e_{ij}, f_{ij} are coefficient resulted from the arrangement of Eq. (26) to the form of Eq. (27). Equation (27) is then solved using the iterative method of, for example, the successive over relaxation or the conjugate gradient.

After getting the water level from Eq. (27), horizontal flow velocities are then calculated from Eq. (10) and Eq. (25). The vertical flow velocity is directly calculated from the mass continuity equation as follows

$$w_{k-1/2}=w_{k+1/2}+\frac{\left(u^{n+1}{}_{k,i,j}S_{HX\,k,i,j}-u^{n+1}{}_{k,i+1,j}S_{HX\,k,i+1,j}\right)}{\Delta x}$$
$$+\frac{\left(v^{n+1}{}_{k,i,j}S_{HY\,k,i,j}-v^{n+1}{}_{k,i+1,j}S_{HY\,k,i,j+1}\right)}{\Delta y} \quad (28)$$

which is the discretized form of Eq. (3). The calculation is done consecutively from the bottom to the surface layers.

5. The Wetting-Drying Scheme

The wetting-drying scheme implemented is the one from Casulli and Cheng [11]. As the water level and flow velocity are completely calculated, before moving to the next time step, the thickness of the surface layer should be adjusted according to the new water level. The new total water depth $H^{n+1}{}_{i+1/2,j}$ and $H^{n+1}{}_{i,j+1/2}$ at the horizontal location of u and v should be calculated. The side-cell water depths $H^{n+1}{}_{i+1/2,j}$ and $H^{n+1}{}_{i,j+1/2}$ are defined as follows

$$H^{n+1}{}_{i+1/2,j}=\max\left(H_{dry},h_{i+1/2,j}+\zeta^{n+1}{}_{i,j},h_{i+1/2,j}+\zeta^{n+1}{}_{i+1,j}\right) \quad (29)$$

$$H^{n+1}{}_{i,j+1/2}=\max\left(H_{dry},h_{i,j+1/2}+\zeta^{n+1}{}_{i,j},h_{i,j+1/2}+\zeta^{n+1}{}_{i,j+1}\right) \quad (30)$$

If the resulting total water depth is less than H_{dry}, then it is considered as a dry point. Furthermore, the respective friction factor will be assumed as infinity, and therefore the corresponding velocity u or v across the side cell is forced to vanish. The dry point means that the velocity is zero and there is no mass flux until at a later time when H is higher then H_{dry}. Furthermore, a cell is considered as a dry cell when all sides are considered as dry. It should be noted here that Eq. (26) is correctly account for a dry cell. At a dry cell, Eq. (26) is reduced to $\zeta^{n+1}{}_{i,j}=\zeta^{n}{}_{i,j}$, which means that there is no water level fluctuation in a dry cell. This assures the mass conservation requirement without the need of special treatment for the free surface water elevation.

6. Results and Discussion

6.1. Comparison with analytical solution

An analytical solution as proposed by Carrier and Greenspan [21] is compared to the numerical results. The analytical solution for horizontal location of the land-ocean interface is as follows

$$\eta = -\frac{1}{2}u'^2 + AJ_0\left(\frac{4\pi\sqrt{\eta - x}}{T}\right)\cos\left(\frac{2\pi}{T}(t+u')\right), \tag{31}$$

where

$$u' = -\frac{4AJ_1\left(\frac{4\pi\sqrt{\eta - x}}{T}\right)}{\alpha}\sin\left(\frac{2\pi}{T}(t+u')\right), \tag{32}$$

$$\alpha = (1+\eta - x)^{1/2} \tag{33}$$

in which u' is the scaled velocity of the moving interface; A is the scaled amplitude; T is the scaled period; t is the scaled time; and η is the scaled free surface elevation from the mean. The scaling changes η to have value the same as the scaled horizontal position. Two parameter in the numerical model, i.e., maximum depth for dry condition H_{dry} and bottom friction coefficient C_D, are not found in the analytical solution. Therefore, the two parameters should be varied to get the best agreement with the analytical solution.

6.1.1. Linear case 1

In this case, the bottom has a linear slope, undisturbed length of 20 km, bathymetric depth at the open sea of 5 m, grid spacing of 250 m, time step of 10 second, tidal amplitude of 0.25 m, tidal period of 12 hours, and simulation time of 4 tidal periods. The base value of H_{dry} and C_D are 0.01 m and 0.001 respectively. Starting from the base value, the two parameters are then varied to get the best agreement with the analytical solution. Comparison between numerical and analytical solution for the location of the land-ocean interface are shown in upper panel of Fig. 4. The numerical solution agrees well with the analytical solution with the averaged error of 1.415%. At the first three tidal periods, the numerical solution has not reached the equilibrium because the computation starts from cold condition. Numerical solution using the base parameter lags behind that of the analytical solution. Improvement is achieved when C_D is set to smaller value of 0.0001. Setting H_{dry} and C_D to 0.01 m and 0.0001 respectively results in the smallest averaged discrepancy from the analytical solution, i.e., 0.797%.

6.1.2. Linear case 2

Besides its steeper bottom slope, the linear case 2 is similar as the linear case 1. The difference with linear case 1 is that linear case 2 has undisturbed length of 18 km and bathymetric depth at the open sea 6 m. The other simulation parameters are the same as linear case 1. Comparison between numerical and analytical solution for the location of the land-ocean interface are shown in the lower panel of Fig. 4. Using the base parameter values, the numerical solution deviates considerably from the analytical solution as much as 7.752%. The best agreement in comparison with the analytical solution is achieved when H_{dry} and C_D are set to 0.05 m and 0.000001

respectively with the averaged error of 1.401%. The result of linear case 2 shows the numerical model capability in modelling large inundation area. Using the same parameters value, more pronounced discrepancy from the analytical solution than that of the linear case 1 is observed. Linear case 2 experiences higher friction due to the higher number of cells that are covered by the intertidal area. Flow of water is dragged greatestly when the water depth reaches the minimum, H_{dry}, and the friction from each cell is accumulated over an intertidal period.

The numerical results of both linear case 1 and linear case 2 are not smooth (saw-tooth behaviour in the time-histories), which is normal due to the step-like representation of bottom topography. Smaller grid spacing should be used to obtain a smoother behaviour of the numerical solution. However, smaller grid spacing requires smaller time step to get stable calculation, which decreases the efficiency of calculation. A numerical experiment is required to get the required accuracy while maintaining the efficiency.

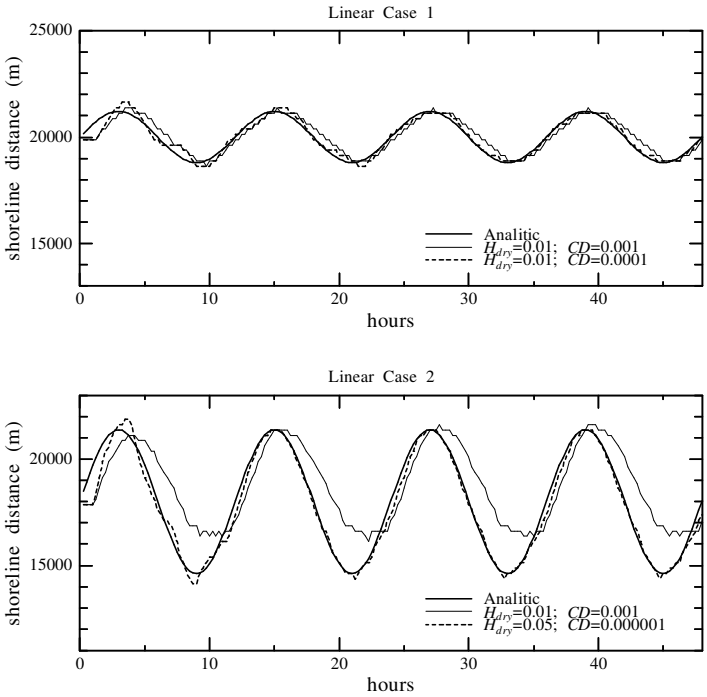

Fig. 4. Comparison of Land-ocean Interface Resulted from Numerical and Analytical.

6.2. Application to Segara Anakan

Segara Anakan, Fig. 5, is a shallow lagoon system that is connected to the ocean by two tidal inlets, in the west and in the east. Nusakambangan Island is in the south protecting the lagoon from waves of the Indian Ocean. Three main rivers, i.e., the Citanduy, the Cikonde, and the Cimeneng, discharge their water into the lagoon. The tidal levels extensively alter the environment of the lagoon through the mechanism of wetting-drying causing large change of inundation areas between low and high tide [22]. This characteristic makes it suitable for testing the model.

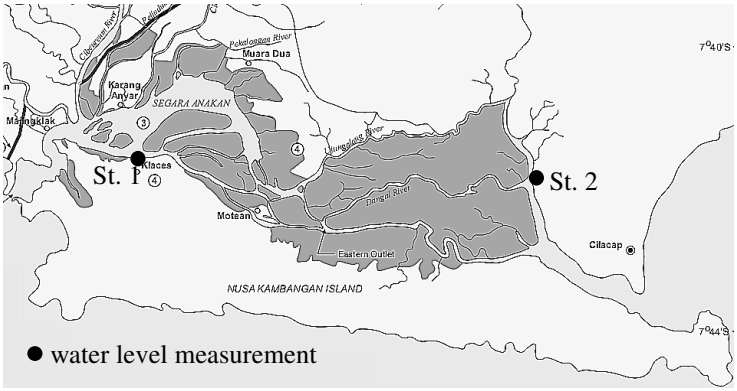

Fig. 5. Segara Anakan and Location of Two Water Level Measurement Stations.

The simulation was conducted over 750×300 grids resulting in uniform meshes size of 40 m. Four layers were used as vertical discretization. The time step was set to 5 s to meet the stability requirement. The period of calculation was 6 days using the boundary conditions of the tidal level at the two tidal inlets. The Citanduy River was assumed to have constant flow discharge of 80 m^3/s. The flow discharges of the other two main rivers, i.e., the Cikonde and the Cimeneng, were assumed to behave similar with the discharge of the Citanduy. Their discharges were obtained from the Citanduy's after multiplying it with the ratio between each catchment's area and that of the Citanduy. Friction coefficient was set to 0.2 for regions above the mean sea level and set to 0.001 for the otherwise. The higher friction coefficient represents the higher friction effect due to mangrove vegetation in the study area.

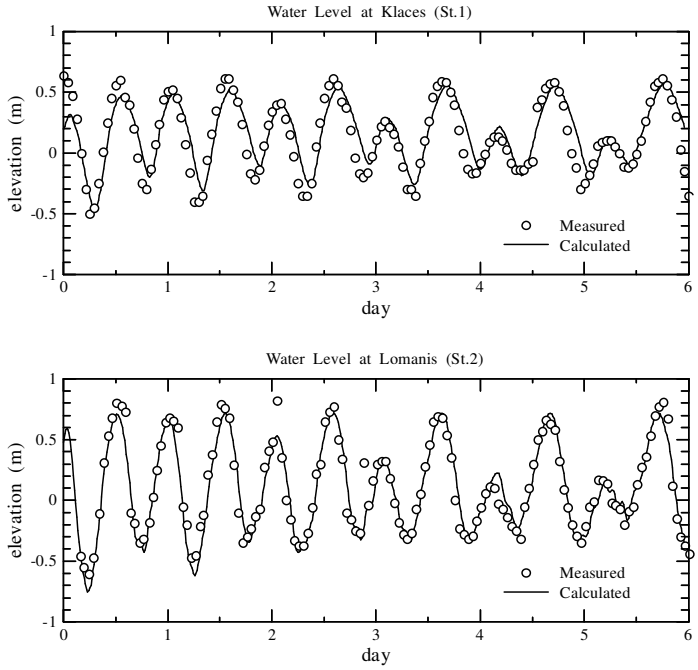

Fig. 6. Water Level at Two Measurement Stations.

Water levels at two locations, Klaces (St.1) in the west and Lomanis (St.2) in the east, were used to validate the calculation results. Figure 6 shows the results of the validation in which the water level could be calculated to match that of the measurements. Compared to water level at St.2, the water level at St.1 fluctuates in lower range due to the damping effect of shallow bathymetry and mangrove vegetation. The simulation covers the large change of inundation area between the flood tide and the ebb tide (Fig. 7).

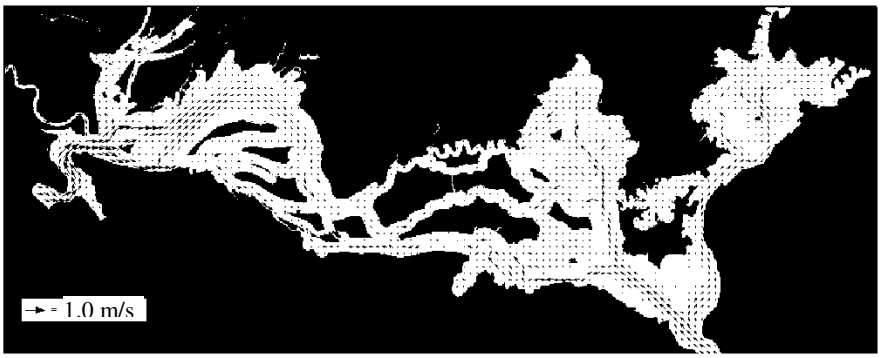

(a)

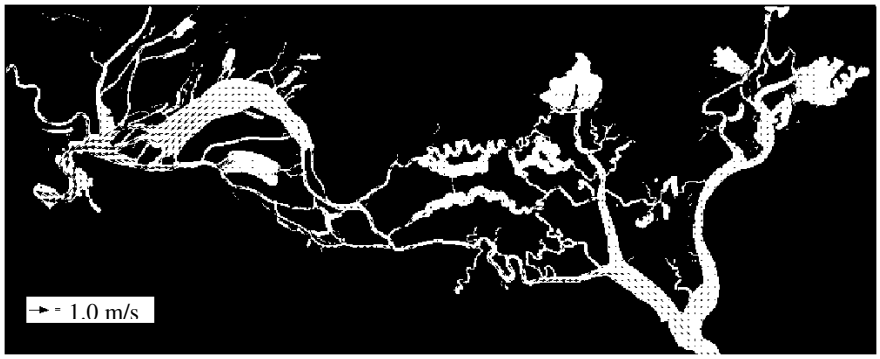

(b)

Fig. 7. Snapshots of Inundation Areas, which are Colored in White, Simulated at Times of a) Flood Tide and b) Ebb Tide.

7. Conclusions

A wetting-drying scheme of Casulli and Cheng [11] is successfully implemented into a three-dimensional shallow water flow numerical model. Comparison with analytical solution shows good agreement. The agreement was achieved after altering two parameters of the maximum depth for dry condition H_{dry} and the bottom friction coefficient C_D. The two parameters act as calibration parameters and they should be adjusted to match the solution. As a rough guidance of choosing the appropriate values of H_{dry} and C_D, a relationship between the two parameters can be found elsewhere [23]. Application to Segara Anakan was also carried out and it shows the numerical model capability in simulating the real condition. The numerical model has

benefit from the efficient calculation of the Sato's model [10] and from the inherent capability of modelling the wetting-drying process as in Casulli and Cheng [11].

Acknowledgments

This work was supported by The Incentive Program of The Ministry of Research and Technology, Indonesia. Peter Holtermann and Tim Jennerjahn let us to use their bathimetry data of Segara Anakan. Aryoto, Indra, Fadly, and Meilani, students of Civil Engineering Department, Universitas Jenderal Soedirman helped us in measuring the water level data of Segara Anakan.

References

1. James, I.D. (2002). Modelling pollution dispersion, the ecosystem and water quality in coastal waters: a review. *Environmental Modelling & Software*, 17(4), 363-385.
2. Blumberg, A.F.; and Mellor, G.L. (1987). A description of a three dimensional coastal ocean circulation model. In: Heaps, N.S. (Ed.), *Three-Dimensional Coastal Ocean Models*. AGU, Washington, DC, USA, 4, 1-16.
3. Haidvogel, D.B.; Arango, H.G.; Hedstrom, K.; Beckmann, A.; Malanotte-Rizzoli, P.; and Shchepetkin, A.F. (2000). Model evaluation experiments in the North Atlantic Basin: simulations in nonlinear terrain-following coordinates. *Dynamics of Atmospheres and Oceans*, 32(3-4), 239–281.
4. Iskandarani, M.; Haidvogel, D.B.; and Levin, J.C. (2003). A three dimensional spectral element model for the solution of the hydrostatic primitive equations. *Journal of Computational Physics*, 186(2), 397–425.
5. Oey, L.Y. (2005). A wetting and drying scheme for POM. *Ocean Modelling*, 9(2), 133–150.
6. Oey, L.Y. (2006). An OGCM with movable land-sea boundaries. *Ocean Modelling*, 13(2), 176-195.
7. Leclerc, M.; Bellemare, J.F.; Dumas, G.; and Dhatt, G. (1990). A finite element model of estuarian and river flows with moving boundaries. *Advances in Water Resources*, 13(4), 158–168.
8. Sampson, J. (2009). A numerical solution for moving boundary shallow water flow above parabolic bottom topography. *Australian and New Zealand Industrial and Applied Mathematics Journal*, 50 (CTAC2008), C898-C911.
9. Gallardo, J.M.; Parés, C.; and Castro, M. (2007). On a well-balanced high-order finite volume scheme for shallow water equations with topography and dry areas. *Journal of Computational Physics*, 227(1), 574-601.
10. Sato, K.; Matsuoka, M.; and Kazumitsu, K. (1993). Efficient calculation method of 3-D tidal current. *Proceedings of Coastal Engineering*, JSCE, 40, 221-225 (in Japanese).
11. Casulli, V.; and Cheng, R.T. (1992). Semi-implicit finite difference methods for three-dimensional shallow water flow. *International Journal for Numerical Methods in Fluids*, 15(6), 629-648.

12. Purwanto, B.S.; Tanaka, H.; Kanayama, S.; Takasaki, M.; and Yamaji, H. (2007). Numerical study on water exchange mechanism in Nagatsura-ura Lagoon. *Annual Journal of Coastal Engineering JSCE*, 54, 1016-1020.
13. Watanabe, K.; Tanaka, H.; Kanayama, S.; and Purwanto, B.S. (2009). Influence of tidal inlet depth on water level response and salinity intrusion in a Lagoon. *Annual Journal of Coastal Engineering JSCE*, 56, 416-420.
14. Balzano, A. (1998). Evaluation of methods for numerical simulation of wetting and drying in shallow water flow models. *Coastal Engineering*, 34, 83-107.
15. Casulli, V.; and Walters, R.A. (2000). An unstructured grid, three-dimensional model based on the shallow water equations. *International Journal for Numerical Methods in Fluids*, 32(3), 331-348.
16. Lynch, D.R.; and Werner, F.E. (1987). Three-dimensional hydrodynamics on finite elements. Part I: Linearized harmonic model. *International Journal for Numerical Methods in Fluids*, 7(9), 871-909.
17. Lynch, D.R.; and Werner, F.E. (1991). Three-dimensional hydrodynamics on finite elements. Part II: Non-linear time-stepping model. *International Journal for Numerical Methods in Fluids*, 12(6), 507-533.
18. Arakawa, A.; and Lamb, V.R. (1977). Computational design of the basic dynamical processes if the UCLA general circulation model. *Methods of Computational Physics*, 17, 174-264, Academic Press.
19. Ramming, H.G.; and Kowalik, Z. (1980). *Numerical modelling of marine hydrodynamics*. Elsevier Scientific Publishing Company.
20. Griffies, S.M.; Boning, C.; Bryan, F.O.; Chassignet, E.P.; Gerdes, R.; Hasumi, H.; Hirst, A.; Treguier, A.; and Webb, D. (2000). Developments in ocean climate modeling. *Ocean Modelling*, 2(3-4), 123-192.
21. Carrier G.F.; and Greenspan H.P. (1958). Water waves of finite amplitude on a sloping beach. *Journal of Fluid Mechanics*, 4(1), 97-109.
22. Holtermann, P.; Burchard, H.; and Jennerjahn, T. (2009). Hydrodynamics of the Segara Anakan lagoon. *Regional Environmental Change*, 9(4), 245-258.
23. Purwanto, B.S.; Nastain; and Widiyanto, W. (2010). Assessment of a hydrodynamic numerical model with wetting-drying capability. *Proceedings of Japan - Indonesia Workshop on Estuary and Climate Change*, Indonesia.